

TWO YEARS OF ACTS PROPAGATION STUDIES IN ALASKA

Charles E. Mayer and Bradley E. Jaeger
 Electrical Engineering Department
 University of Alaska Fairbanks
 P.O. Box 755900
 Fairbanks, AK 99775-5900

L INTRODUCTION

The Alaska ACTS Propagation Terminal (APT) is located on top of the engineering building on the University of Alaska Fairbanks campus. The latitude and longitude of the site are 64° 51' 28" N and 147°48'59" W. The geometrical elevation angle to ACTS is 7.97°. Including a normal atmospheric refractivity, the elevation angle increases to 8.10°. The azimuth angle to ACTS is 129.36°. The terminal is located at 580 feet above mean sea level. The site is located in ITU-R rain zone C and Crane global model zone B 1. ACTS transmits vertical polarization beacons at 27.505 and 20.185 GHz. At the APT the polarization tilt angle is 19.4° rotated CCW with respect to vertical when looking toward the satellite. The beacons are transmitted in a CONUS pattern. The ACTS beacon footprint at the Alaska APT site is 9 dB down from the transmission pattern peak at 27.505 GHz and 11dB down from the pattern peak at 20.185 GHz. We will henceforth refer to the beacon frequencies as 27.5 (or 27) and 20.2 (or 20) GHz for the sake of brevity.

11. FAIRBANKS WEATHER

An understanding of the weather in Fairbanks is pertinent to understanding the displayed results. Fairbanks has very cold and very dry winters. The months November through March can be considered winter, where the only form of precipitation is snow, usually very dry. The transition months of September, October, and April can experience rain, wet snow, or possibly some dry snow. Snow does not greatly attenuate microwave signals. Rain is normally experienced May through September. The annual average precipitation in Fairbanks is 11.0 inches, as shown in Table L below.

Table L Annual Weather Statistics in Fairbanks by Month

Month	Precipitation (Inches)	No. of Days with ≥ 0.1 in. Precipitation	Mean Minimum Temperature, °C	Mean Maximum Temperature, °C
January	0.69	2.1	-28.9	-18.9
February	0.58	1.9	-26.1	-12.7
March	0.41	1.1	-20.6	-5.0
April	0.25	0.6	-8.8	4.9
May	0.71	2.0	2.2	14.8
June	1.42	3.2	7.7	21.0
July	1.90	4.0	9.3	22.2
August	2.03	4.2	6.6	18.8
September	1.26	2.6	1.1	12.1
October	0.73	1.9	-7.8	1.1
November	0.48	1.6	-20.6	-11.1
December	0.55	1.8	-27.8	-18.9
Yearly Total	11.00	27.0	-9.4	2.2

III. MONTHLY AND YEARLY ATTENUATION AND RAIN RATE CDFs

The major experimental results of the measurement campaign are the total attenuation and rain rate. The cumulative distribution function (CDF), which is also called an empirical distribution function (EDF), is the primary method of displaying the experiment results. The abscissa on the attenuation CDF plot is total attenuation in dB ranging from -5 to 30 dB, and the ordinate is percentage time the attenuation is greater than the abscissa ranging from 0.001 to 100%. The abscissa on the rain rate CDF plot is rain rate in mm/hr, and the ordinate is percentage time the rain rate is greater than the abscissa. The attenuation and rain rate CDFs are presented for each month and also on a yearly basis. These CDFs are presented time sequentially in the appendix of this document. The attenuation CDFs include both beacon and radiometer distributions for both 20.2 and 27.5 GHz. The monthly attenuation CDFs display results that parallel the discussion of Fairbanks weather above. The CDFs for the cold, dry winters exhibit very low attenuation. The CDFs for the warmer summers exhibit larger percentages of attenuation at a few dB (1 -4 dB). This attenuation is due to gaseous absorption. At a low elevation angle, the Fairbanks-ACTS link propagates through about 8 airmasses of atmosphere, where one airmass is the amount of atmosphere integrated to zenith. The summer CDFs also exhibit larger attenuation at the lower percentages. This attenuation is due to hydrometers, mostly rain. The monthly rain rate CDFs clearly correspond to the attenuation measured during that month. The large variability in these CDFs from month to month, the similarity of each month from year to year, and the predictable trends from the above Fairbanks weather discussion indicate the importance of viewing attenuation statistics on a monthly basis. First we will discuss some overall features of these CDFs.

A. Total Attenuation CDFs

Several features must be explained to help interpret the results displayed in these attenuation CDFs. Due to the extra pattern footprint loss in Alaska and the limited dynamic range of the AFT, the total attenuation with respect to free space can be accurately measured to a total attenuation level of approximately 18 dB with a sufficiently high signal-to-noise ratio, so that the attenuation value given is accurate. Values of attenuation greater than this threshold are given the value of 35 dB by the preprocessing program and displayed as 30 dB on the CDFs. Thus an attenuation value of 24 dB would be displayed as 30 dB, as would an attenuation value of 40 dB. This method of binning values was chosen so that the total time of attenuation greater than the measurement threshold would be properly accounted for. This tends to flatten out the tails of attenuation CDFs. This is not the shape that the CDFs would show were the measurement dynamic range larger. Values on the CDFs greater than 15 to 20 dB therefore do not accurately represent measured data and should not be taken as valid measurements.

Figure 1 shows the yearly attenuation CDFs for year 1 and year 2. Both the 20 and 27 GHz beacons are displayed. The attenuation displayed is the total attenuation, including gaseous absorption, rain attenuation, snow attenuation, scintillation, antenna wetting, and any other hydrometeor-caused attenuation. The 20.2 GHz beacon experiences more gaseous attenuation and hence has larger attenuation at the lower attenuation levels. The 27.5 GHz beacon experiences more hydrometer attenuation and hence has larger attenuation at the higher attenuation levels. The crossover point of the two frequency attenuation curves is clearly at the 4 dB and 2% point. The 20.2 GHz beacon is reasonably close to the atmospheric water vapor absorption line at 22.2 GHz. The 27.5 GHz beacon, although higher in frequency, is farther from this absorption line and experiences less specific attenuation due to water vapor. By including year 1 and year 2 together in Figure 1, a measure of the variability between these two years can be readily seen. A word of

caution must be given when interpreting these CDF's. The average of these two years cannot be taken as the "average" year in Fairbanks. Many more years would need to be included to give an accurate assessment of the average year. Thus although these curves show points and narrow lines, it is not accurate to use these curves as an average attenuation.

Often a communications system must be designed to meet worst month statistics. Figure 2 shows the worst month envelope of attenuation. This curve was created comparing equi-attenuation values and selecting the highest percentage time at each of those levels. It should be noted that the 3 summer months of June, July and August were the only months that contributed to this worst month CDF.

II., Rain Rate CDFs

Rain is the only form of precipitation measured in the ACTS experiment; precipitation from snow is not measured. The yearly and monthly rain rate CDFs are shown in the appendix. It is interesting to note that year 1 had a higher percentage of larger rain rate events, but year 2 was a wetter year, demonstrating higher attenuation than year 1. A comparison of the rain rate in year 1, year 2 and the ITU-R rain zone C model is presented in Table II, below. The rain rate measurements were taken with a Young's capacitive rain gauge. The gauge has proven troublesome. Several sites have replaced the capacitive rain gauge with a tipping bucket rain gauge. We have used an optical gauge in conjunction with the capacitive gauge. The two gauges yield similar results for rain rates larger than several mm/hr. The capacitive gauge is noisy, often indicating rain when there is no rain present. We used the optical gauge to remove these anomalous rain indications, and then calculated monthly statistics based upon the amended capacitive gauge numbers.

Table II. Rain Rate in mm/hr

	0.1 %	0.01 %	0.001 %
Year 1 measurements	4.5	9	40
Year 2 measurements	4.5	10	20
ITU-R zone C model	5	15	42

IV. SCINTILLATION ANALYSIS

The impact of rain-induced attenuation on satellite-earth communication links at frequencies above 10 GHz is generally predominant. However, for the design of low margin systems, especially those at high frequencies and low elevation angles, scintillation effects must be properly estimated to accurately complete the link budget.

Scintillations are rapid fluctuations (on the scale of a few seconds to tens of seconds) in the magnitude of the received beacon level. The turbulence in the troposphere is concentrated in the planetary boundary layer, the moist layer of air ranging from the earth's surface up to a height of 1 to 1.5 km. Variations in humidity, pressure, temperature and magnitude and scale size of turbulence in the troposphere change the refractive index along the propagation path. These small scale and time varying perturbations cause amplitude, phase, and angle of arrival fluctuations, known as scintillations. The signal, after propagation through this turbulent layer, can be considered a random variable. This random variable can be described by its probability density function and its power spectrum. Theoretical studies [Tatarskii, Strohbehn, Ishimaru] yield models of these characteristic parameters based upon meteorological parameters that cannot be measured. The lack of knowledge of these meteorological parameters along the propagation path length

has led to the development of semi-empirical models representing the magnitude and characteristics of scintillations.

The intensity of the scintillations must be accurately portrayed by a measurement unit. The scintillation process is assumed to be a zero-mean process with fluctuations about that mean. The fluctuations can be represented in terms of their root mean square, or rms. Since the mean of the process is zero, the rms can be represented by the standard deviation of the process.

The measure of the intensity of scintillation used will be the standard deviation of the log amplitude of the received signal, that is, the standard deviation of the received signal in decibels. The time duration of the standard deviation calculation will be one minute.

A. Time Series Analysis

Figure 3 shows the received 27.5 GHz beacon level over a period of 10 minutes on August 16, 1994. Large variations of the received beacon level are apparent from this figure. The time behavior of scintillations is demonstrated on this summer day of large scintillations. The day was humid and warm, with a light wind and full sky cover. An expanded view of this period is shown in Figure 4, which covers 1 minute of time on this day. Note that the 20.2 and 27.5 GHz beacons are both displayed, and are closely correlated over most of the time. There is about a 2 dB difference for several seconds. Also of note is the rapid rise of received beacon level in seconds 20 through 25. Both frequencies experience a 5 dB rise in 6 seconds. The mean level of these signals is about -13 dB (the scale is a relative scale), so that the signal enhancement is only about 3 dB above the nominal level. Signal attenuation is thought of as the major impairment to communications systems. However, signal enhancements can also cause problems, especially in multi-carrier transponder operation, where the input power must remain below the nonlinear threshold. If too much input power is supplied, the transponder becomes more nonlinear, producing intermodulation (IM) distortion, which can greatly reduce the overall C/N. Figure 5 is included to present another time series view of scintillation in a representative minute; this example is minute 38 in the hour. Again the behavior of both beacons is highly correlated, with only intervals of several seconds where they differed by several dB. Also note the rapid decrease of 3 to 4 dB during the 3 seconds near the end of the minute. During this hour on August 16, 1994 the beacons experienced large scintillations, as in most of the day. The distribution of scintillations will be studied using PDFs (probability density functions) of one minute standard deviation in several time durations.

B. PDFs

The APT samples each beacon (and each radiometer) once a second. Scintillations were studied by calculating the standard deviation in one minute periods of received beacon data (60 samples at each frequency). The standard deviations, measured in dB, were binned in 0.05 dB width bins. The number of calculated standard deviations (i.e., the number of seconds) in each bin were tabulated, forming a histogram distribution of the number of seconds of scintillation standard deviation at each bin dB value. These histogram distributions were produced over a 1 hour time period, over a 1 day time period, and over a 1 month time period. The nesting hour, day, and month were 18-19 GMT, 16th, and August 1994. The number of minutes at each standard deviation value bin were plotted in PDFs, or probability density functions. Figure 6 shows the PDF for one hour of standard deviation values. The time period is 18-19 GMT on August 16, 1994. The abscissa of the plot is one minute standard deviations in dB. The ordinate is the probability of occurrence, displayed on a logarithmic axis. For example, there was a 10% probability of the standard deviation being 0.75 dB for the 20.2 GHz beacon and about an 8% probability of the standard deviation being 0.75 dB for the 27.5 GHz beacon. It is clear that the scintillations were large during the hour, as the standard deviation was less than 0.5 dB for only a

few percent of the time for the 20.2 GHz beacon and less than 0.7 dB for a small percentage of time for the 27.5 GHz beacon. The standard deviations for the entire day of August 16, 1994 are shown in Figure 7. It is clear that there were many times of lower magnitude standard deviations over the whole day as compared to the one hour displayed in Figure 6. Also of note is that there were larger standard deviation values for a small percentage of the time. Finally, the PDF of the standard deviations for the entire month of August 1994 is presented in Figure 8. Again the distribution tends to move toward lower values of standard deviations.

C. Scintillation Standard Deviation

increasingly, models for attenuation due to scintillation, gases, and clouds are becoming important for low margin satellite applications. Total fade distributions have applications in determining link margins and in determining service quality [Salonen, Matsudo]. Models for the fading due to scintillation incorporate the standard deviation of signal amplitude (σ_x) in two ways. First, the formulation of the long term cumulative distribution (CDF) of scintillation log amplitude (χ in dB) is undertaken by assuming two distributions. If a conditional distribution of χ given σ_x and a distribution for σ_x are given, the CDF of log amplitude can be found by integrating over the product of these two distributions [Allnutt]. Second, the models for fading due to scintillation incorporate a prediction of the mean standard deviation of signal amplitude based on the local wet refractivity. The authors present the first year of the standard deviation of signal amplitude. They found that for the first year of observation the standard deviation of signal amplitude was bounded by both the CCIR model and the Karasawa model. They present a typical probability density function for the standard deviation of signal amplitude and measured prediction equations for the mean standard deviation of signal amplitude from wet refractivity for the first year.

D. Two Standard Probability Density Functions of Standard Deviation

Two models are generally accepted for the standard deviation of signal amplitude, the Karasawa gamma distribution and the Moulsey-Vilar lognormal distribution. These models describe the standard deviation of attenuation with rain and gas attenuation effects removed. The equation used to perform this operation [Crane] is as follows:

$$\sigma_x = \sqrt{\text{var}(AFS) - \text{var}(ARD)}, \quad (1)$$

where $\text{var}(AFS)$ is the variance in the free space attenuation, or total attenuation, and $\text{var}(ARD)$ is the variance in the radiometer attenuation channel, which accounts for the rain and gaseous attenuation. The Karasawa gamma distribution [Allnutt] describes the distribution of signal standard deviation using parameters β and ζ that could be related to measurements:

$$f = \frac{\beta^\zeta}{\Gamma(\zeta)} \cdot \sigma_x^{\zeta-1} \cdot \exp(-\beta \cdot \sigma_x) \quad (2)$$

$$\beta = \frac{m}{\sigma_{\sigma_x}^2} \quad \text{and} \quad \zeta = \frac{m^2}{\sigma_{\sigma_x}^2}$$

The mean of the signal standard deviation is equal to m and the variance of the signal standard deviation is $\sigma_{\sigma_x}^2$. This distribution is used to form the CDF of scintillation fading in both the CCIR model and the Karasawa model. Moulsey and Vilar obtained cumulative distributions for signal fading by using a lognormal probability density function for the standard deviation of signal fading [Moulsey]:

$$f = \frac{1}{\sigma_{\sigma} \cdot \sigma_x} \cdot \sqrt{\frac{2}{\pi}} \cdot \exp\left(-\frac{\left(\ln\left(\frac{\sigma_x^2}{\sigma_m^2}\right)\right)^2}{2 \cdot \sigma_{\sigma}^2}\right), \quad (3)$$

where

$$m = \ln(\sigma_m^2) = \text{avg}(\ln(\sigma_x^2)) \text{ and } \sigma_{\sigma} = \text{var}(\ln(\sigma_x^2)).$$

In Fairbanks the authors have obtained measured distributions of signal standard deviation. Statistical K-S tests of these distributions against gamma and lognormal distributions will be presented later in the Proceedings of the IEEE. Typical distributions for each beacon frequency arc shown in Figures 9 and 10.

E. Prediction of Average Signal Standard Deviation from Wet Refractivity

There are two accepted models for predicting an average signal standard deviation, the CCIR model and the Karasawa model. Each model makes a prediction of the signal standard deviation from the average wet refractivity and then scales to frequency, elevation angle, and aperture size. Figures 11 and 12 show the annual variation in average hourly standard deviation at Fairbanks. The data for the first year are below both the CCIR model and the Karasawa model predictions.

Using station parameters from Haystack, Massachusetts, the CCIR model scales to frequency, elevation angle, and aperture size as follows:

$$\sigma_{pre} = \frac{\sigma_{ref} \cdot f^{\frac{7}{12}} \cdot g(x)}{\sin(\theta)^{1.2}} \quad (4)$$

with

$$\sigma_{ref} = 0.0036 + 0.00013 \cdot N_{wet}$$

$$g(x) = \sqrt{3.86 \cdot (x^2 + 1)^{\frac{11}{12}} \cdot \sin\left(\left(\frac{11}{6}\right) \cdot \arctan\left(\frac{1}{x}\right)\right) - 7.08 \cdot x^{\frac{5}{6}}}$$

$$x = 0.00584 \cdot D_{eff}^2 \cdot \frac{k}{L}$$

$$D_{eff} = \sqrt{\eta} \cdot D$$

$$L = \frac{2 \cdot h}{\sqrt{\sin^2(\theta) + \left(\frac{2 \cdot h}{r_e}\right)^2} + \sin(\theta)}$$

$$N_{wet} = \frac{3730 \cdot H \cdot e_s}{e \cdot (273 + t)^2}$$

$$e_s = \frac{5854 \cdot \left(10^{\left(20 - \frac{2950}{273+t}\right)}\right)}{(273 + t)^5}$$

where

- σ_{pre} is the predicted monthly average standard deviation of signal amplitude (dB)
- L is the effective turbulent path length (m)
- h is the turbulence height (m)
- e is the elevation angle
- D_{eff} is the effective antenna diameter(m)
- D is the antenna diameter (m)
- k is the wave number (m⁻¹)
- η is the antenna efficiency
- r_e is the effective earth radius= $8.5 \cdot 10^6$ (m)
- N_{wet} is the wet refractivity (N units)
- e_s is the monthly average saturated water vapour pressure (rob)
- t is the monthly average surface temperature (°C).

The Karasawa model is very similar, scaling from its station parameters at Yamaguchi, Japan, to other frequencies, elevation angles, and aperture sizes. The main theoretical difference between the two models is the scaling with frequency, $f^{7/12}$ versus $f^{0.45}$. Karasawa made the argument that Yamaguchi frequencies fell in between the diffraction region and the geometrical optical region. The diffraction region was assumed to be under the Tatarskii model, $f^{7/12}$, and the geometrical optical region was assumed to be under the Yokoi model, f^0 . The Karasawa model is as follows:

$$\sigma_x = \sigma_{x,ref} \cdot \eta_f \cdot \eta_\theta \cdot \eta_{D_a} \quad (5)$$

with

$$\sigma_{x,ref} = 0.15 + 0.0052 \cdot N_{wet} \quad \eta_f = \left(\frac{f}{11.5}\right)^{0.45} \quad \eta_\theta = \left(\frac{\text{cosec}(\theta)}{\text{cosec}(6.5^\circ)}\right)^{1.3} \quad \theta > 5^\circ$$

$$\eta_{D_a} = \sqrt{\frac{G(D_a)}{G(7.6)}}$$

$$N_{wet} = \frac{3730 \cdot H \cdot e_s}{(273 + t)^2}$$

$$e_s = 6.11 \cdot \exp\left(\frac{19.7 \cdot t}{(t + 273)}\right)$$

$$R = 0.75 \cdot \left(\frac{D_a}{2}\right)$$

$$G(R) = 1.0 - 1.4 \cdot \frac{R}{(\sqrt{\lambda} \cdot L)} \quad \text{for OS } \frac{R}{\sqrt{\lambda} \cdot L} \leq 0.5$$

$$L = \frac{2 \cdot h}{\sqrt{\sin^2(\theta) + \left(\frac{2 \cdot h}{r_e}\right)^2} + \sin(\theta)}$$

where

σ_x is the predicted monthly average standard deviation of signal amplitude (dB)
 $\sigma_{x,ref}$ is the unscaled predicted monthly average standard deviation of signal amplitude (dB)
 N_{wet} is the wet refractivity (N units)
 η_f is the frequency scaling, f is the frequency (GHz)
 η_θ is the elevation angle scaling, θ is the elevation angle
 η_{D_a} is the antenna diameter scaling, D_a is the antenna diameter (m)
 H is the monthly average relative humidity (%)
 c_s is the monthly average saturated water vapour pressure (rob)
 t is the monthly average surface temperature (°C)
 $G(R)$ is the antenna aperture averaging factor
 R is the effective radius of circular aperture (m)
 L is the effective turbulent path length (m)
 h is the turbulence height (2000 m)
 r_e is the effective earth radius= $8.5 \cdot 10^6$ (m).

In Fairbanks the relationship between average hourly standard deviation and wet refractivity, in the first year, was as given in Figure 13 and Figure 14. Additional data will be analyzed before deciding if these relationships are statistically different from the models.

The frequency scaling exponent for the first year was nearly equal to the Karasawa model. The ratio of standard deviations, 1.14, was calculated from an average ratio of standard deviations. The arguments in the average came from interpolating equal percentage points on cumulative distribution functions. Solving the CCIR scaling relation for a :

$$a = \frac{\ln\left(\frac{\sigma(f,\theta)}{\sigma(f_0,\theta_0)}\right) - 1.2 \cdot \ln\left(\frac{\sin(\theta_0)}{\sin(\theta)}\right) - \frac{1}{2} \cdot \ln\left(\frac{G(R)}{G(R_0)}\right)}{\ln\left(\frac{f}{f_0}\right)} \quad (6)$$

Substituting 1.14 for the ratio of standard deviation gives $a=0.44$.

Figure 15 and Figure 16 show the month to month variability in standard deviations. The months of January and August are nominally the months with the smallest and largest scintillation. All other months typically fit between these bounds. Figure 17 shows the one year CDFS of standard deviation and associated power law fits.

v. CONCLUSIONS

The Fairbanks AK APT site is the only APT site with a low elevation angle, This feature allows measurements to be made on a long propagation path length through the atmosphere. Propagation phenomena that are strongly elevation angle dependent include. gaseous absorption and scintillations. The AK APT clearly experiences large amounts of gaseous absorption during the humid summer months, as seen in the total attenuation CDFs. Scintillations have been analyzed and presented in PDFs of their standard deviation. For the month of August 1994, one minute standard deviations were greater than 1.5 dB for 0.02% of the month at 20.2 GHz and for 0.03% of the month for 27.5 GHz. It should be noted that the beacon peak-to-peak variation is significantly larger than the standard deviation. For example, the 10 minute time series of beacon data shown in Figure 3 has a standard deviation of 0.88 dB, whereas the peak-to-peak variations are on the order of 5.0 dB. Two models of signal standard deviation (CCIR and Karasawa), which

quantifies the magnitude of scintillations, were compared to the measured data, with the measured values being significantly less than both models.

REFERENCES

- Allnutt, J. E., Y. Karasawa, and M. Yamada, "A New Prediction Method for Tropospheric Scintillation on Earth-Space Paths," *IEEE Transactions on Antennas and Propagation*, pp. 1608-1614, November 1988.
- Crane, R. K., E-mail Communication.
- Ishimaru, A., *Wave Propagation and Scattering in Random Media*. New York: Academic Press, 1978.
- Matsudo, T. and Y. Karasawa, "Characteristics and Prediction methods for the Occurrence Rate of SES in Available Time Affected by Tropospheric Scintillation," *Electronics and Communications in Japan*, pp. 843-851, December 1990.
- Moulsley, T. J., and E. Vilar, "Experimental and Theoretical Statistics of Microwave Amplitude Scintillations on Satellite Down-links," *IEEE Transactions on Antennas and Propagation*, pp. 1099-1106, November 1982.
- Salonen, E. T., J. K. Tervonen, and W. J. Vogel, "Scintillation Effects on Total Fade Distributions for Earth-Satellite Links," *IEEE Transactions on Antennas and Propagation*, pp. 23-27, January 1996.
- Strohbehn, J. W., "Line-of-Sight Wave Propagation Through the Turbulent Atmosphere," *IEEE Proceedings*, vol. 56, no. 8, pp. 1301-1318, August 1968.
- Tatarskii, V. I., *Wave Propagation in a Turbulent Medium* (translated by R. A. Silverman). New York: McGraw-Hill, 1961.

Fig. 1. AK Yearly Beacon Attenuation (second) EDF

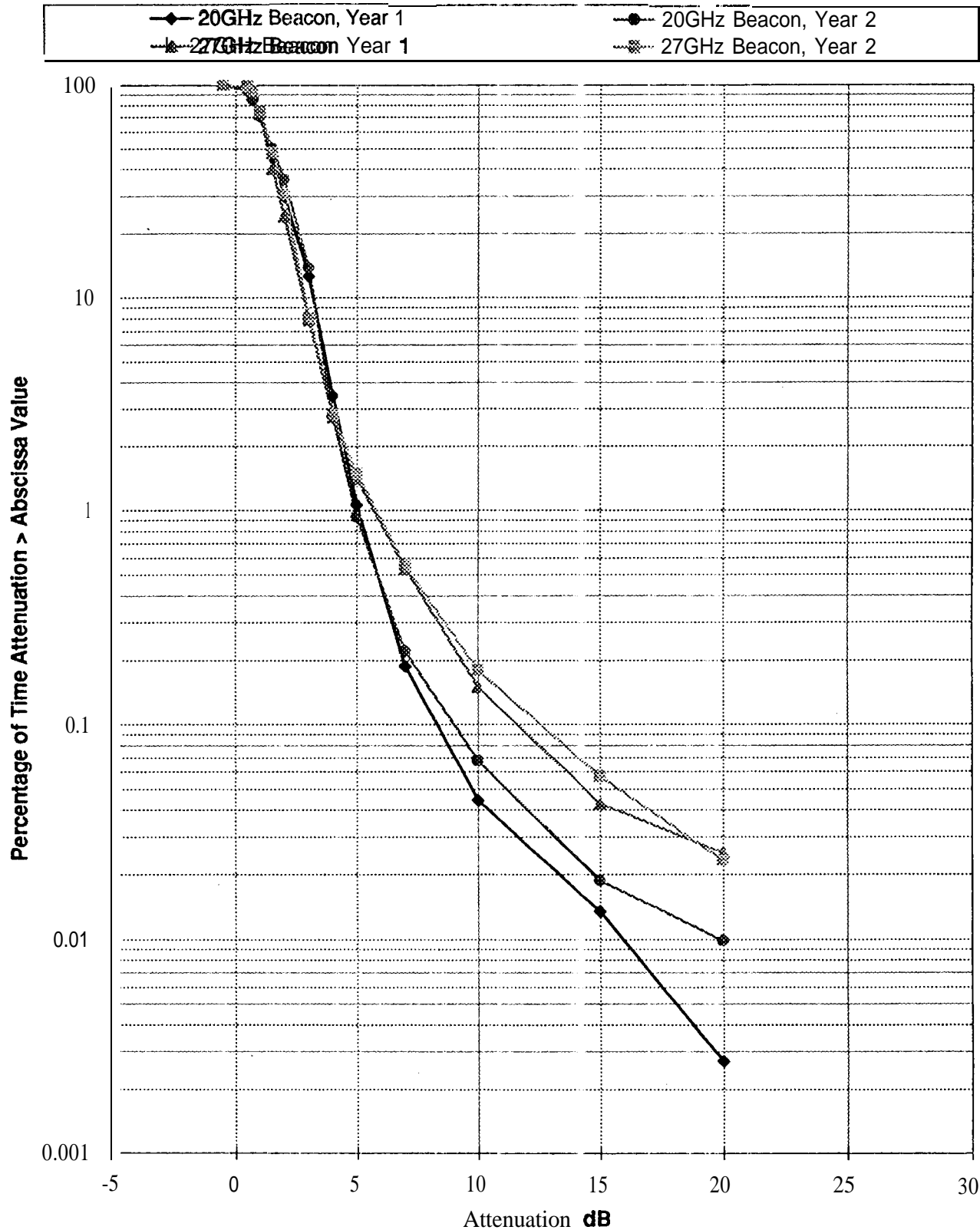


Fig. 2. 2 Year Envelope of Worst Monthly Attenuation (second) EDF

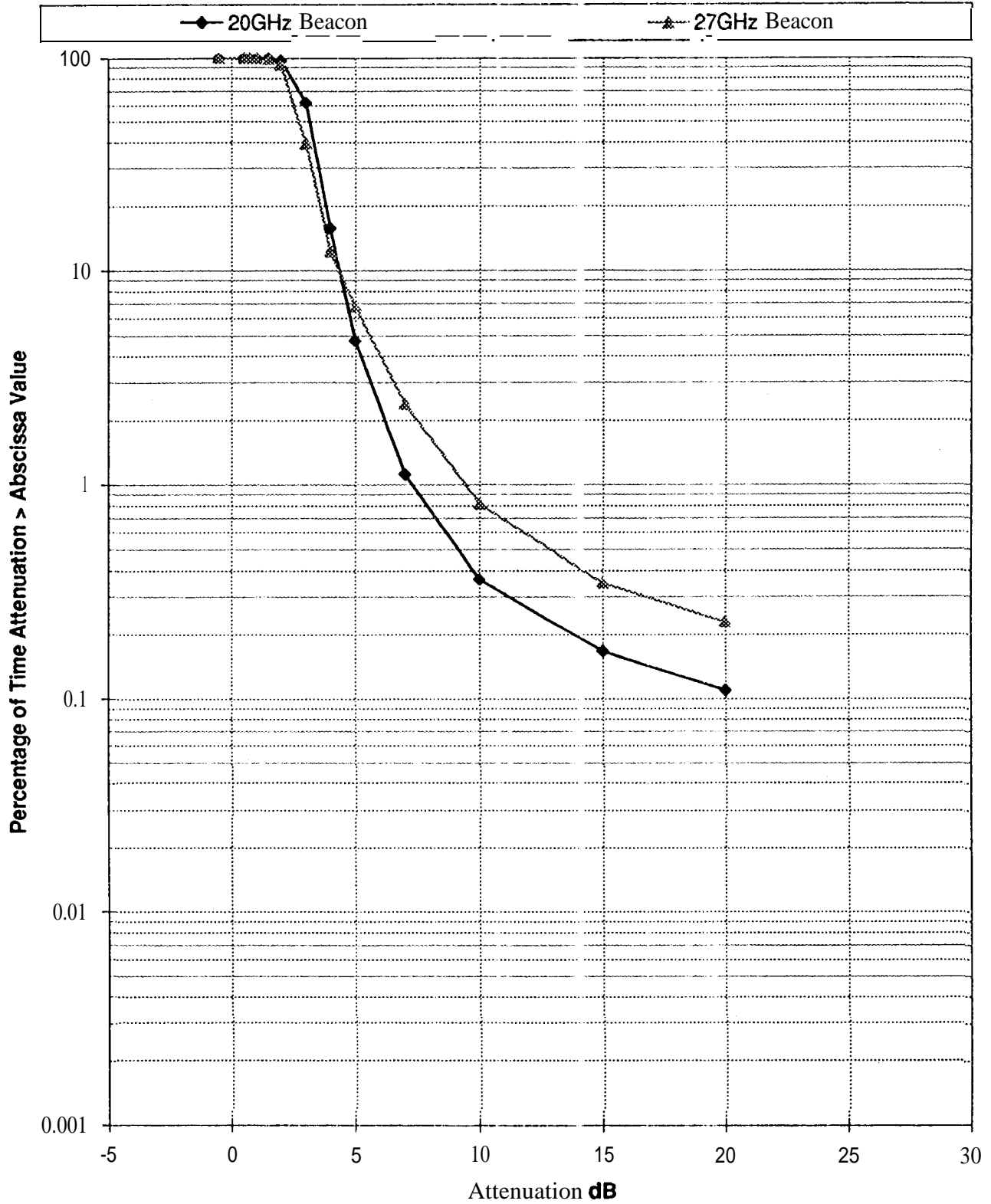


Fig. 3. 27.5 GHz Beacon Levels

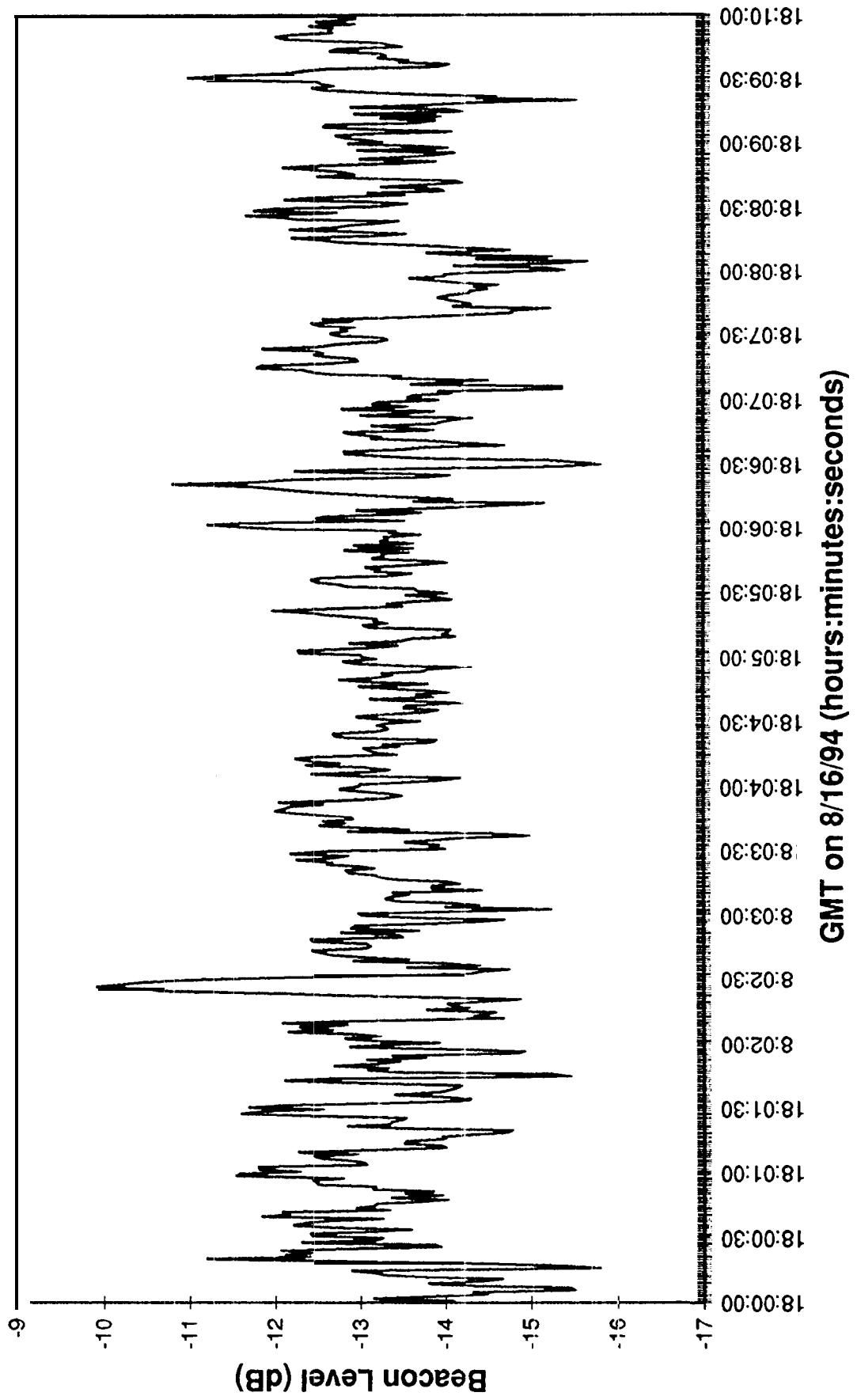


Fig. 4. 20.2 and 27.5 Beacon Levels

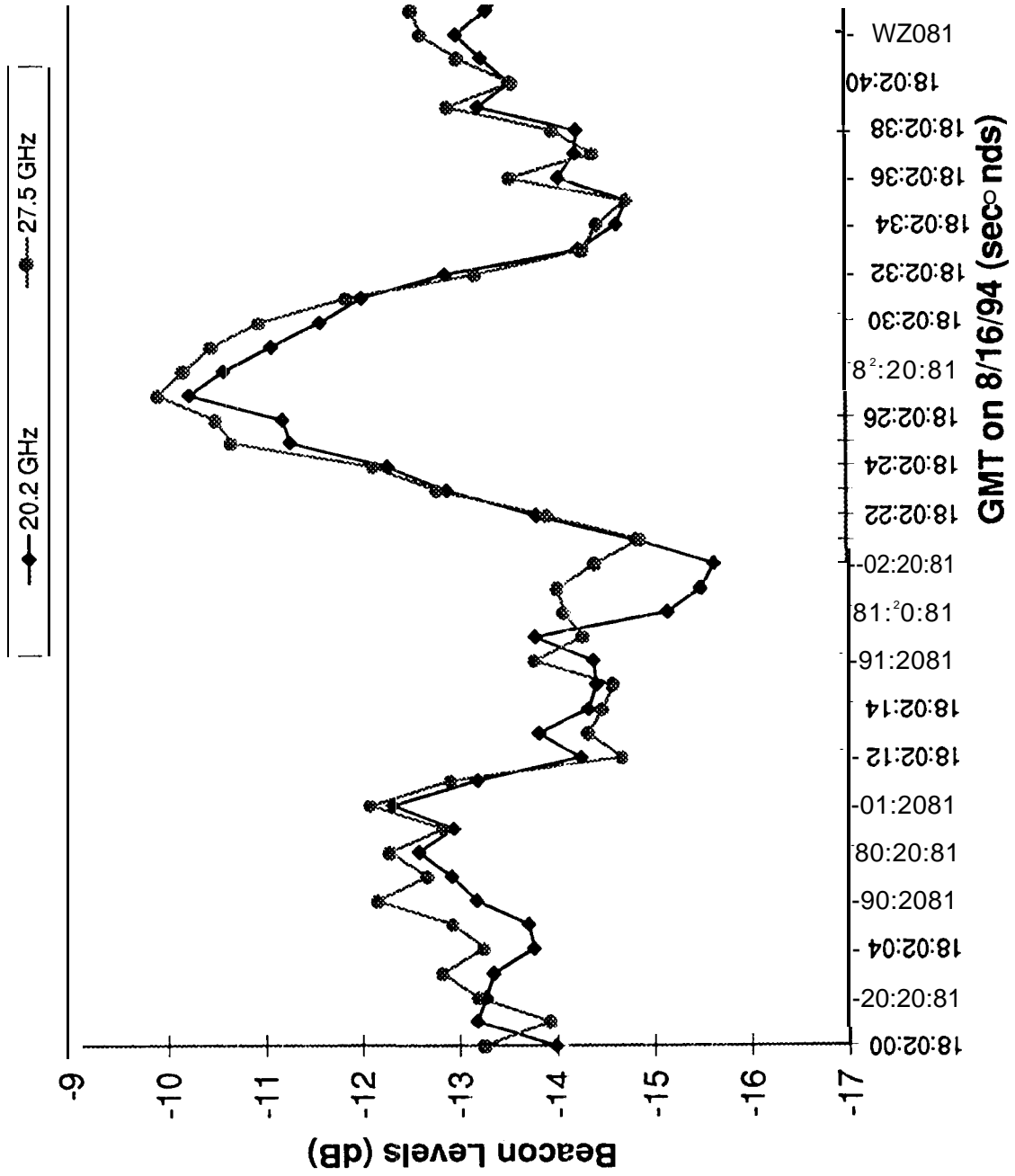
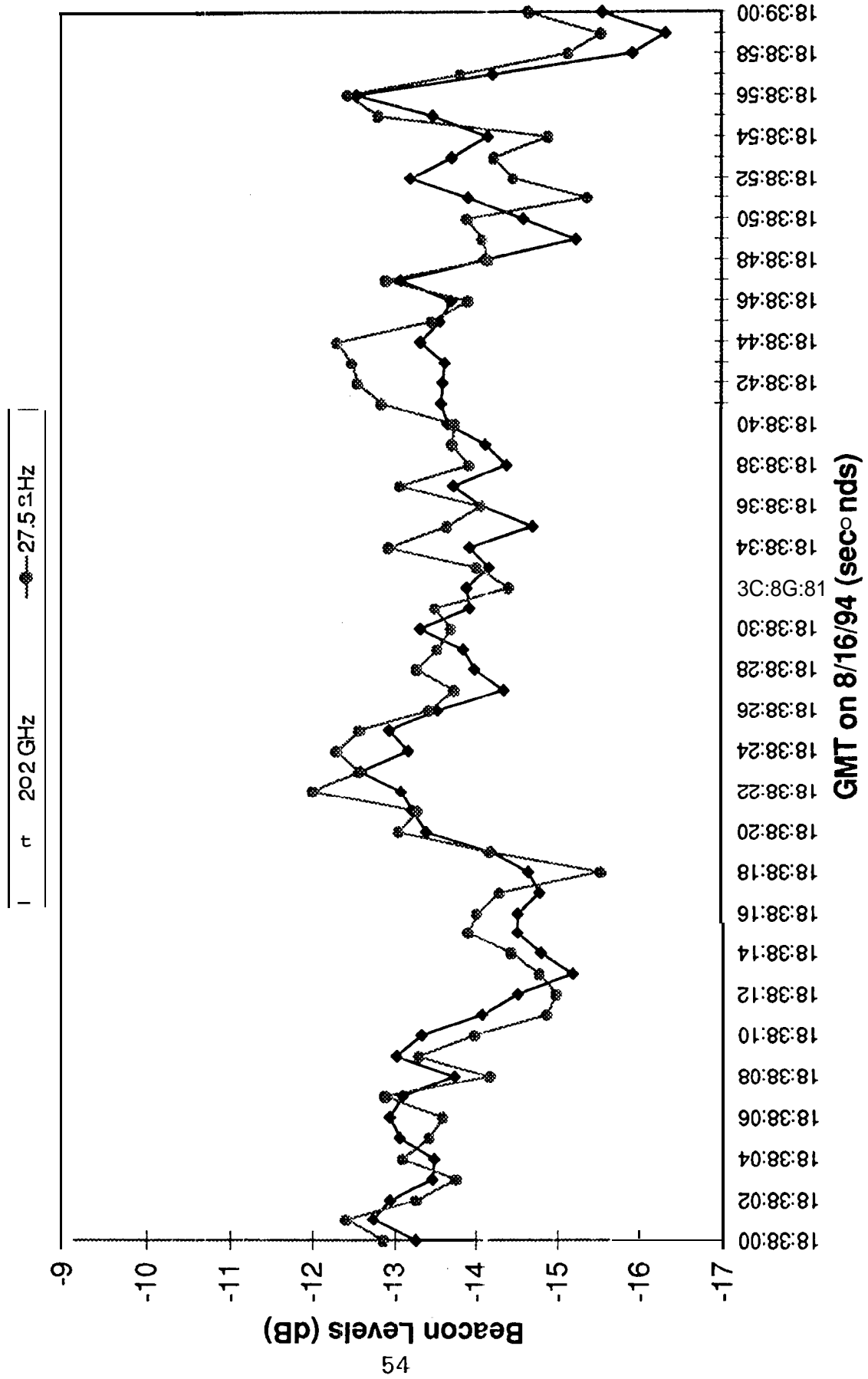


Fig. 5. 20.2 and 27.5 Beacon Levels



**Fig. 6. One Minute Standard Deviation PDF
18-19H GMT 8/1 6/94**

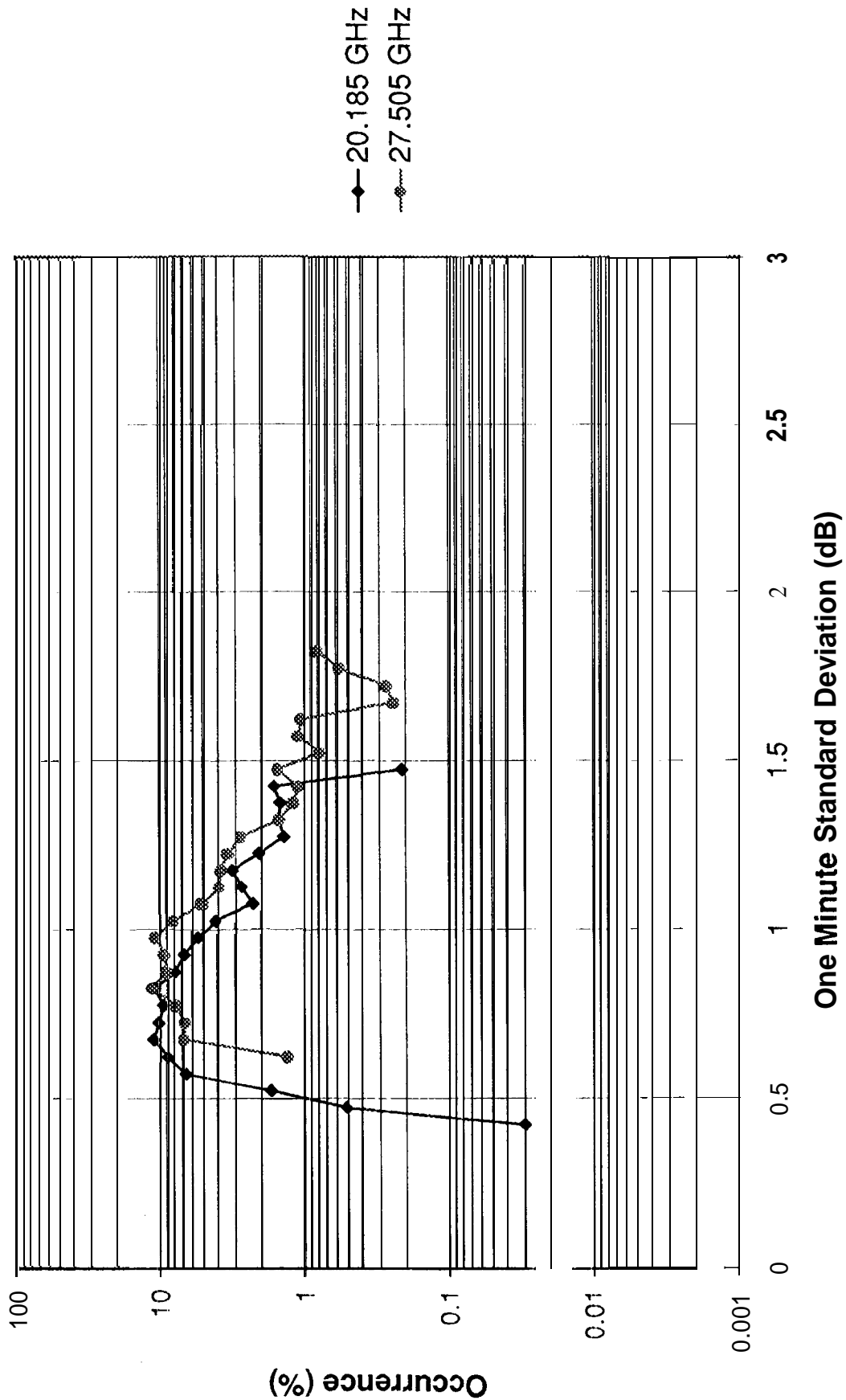
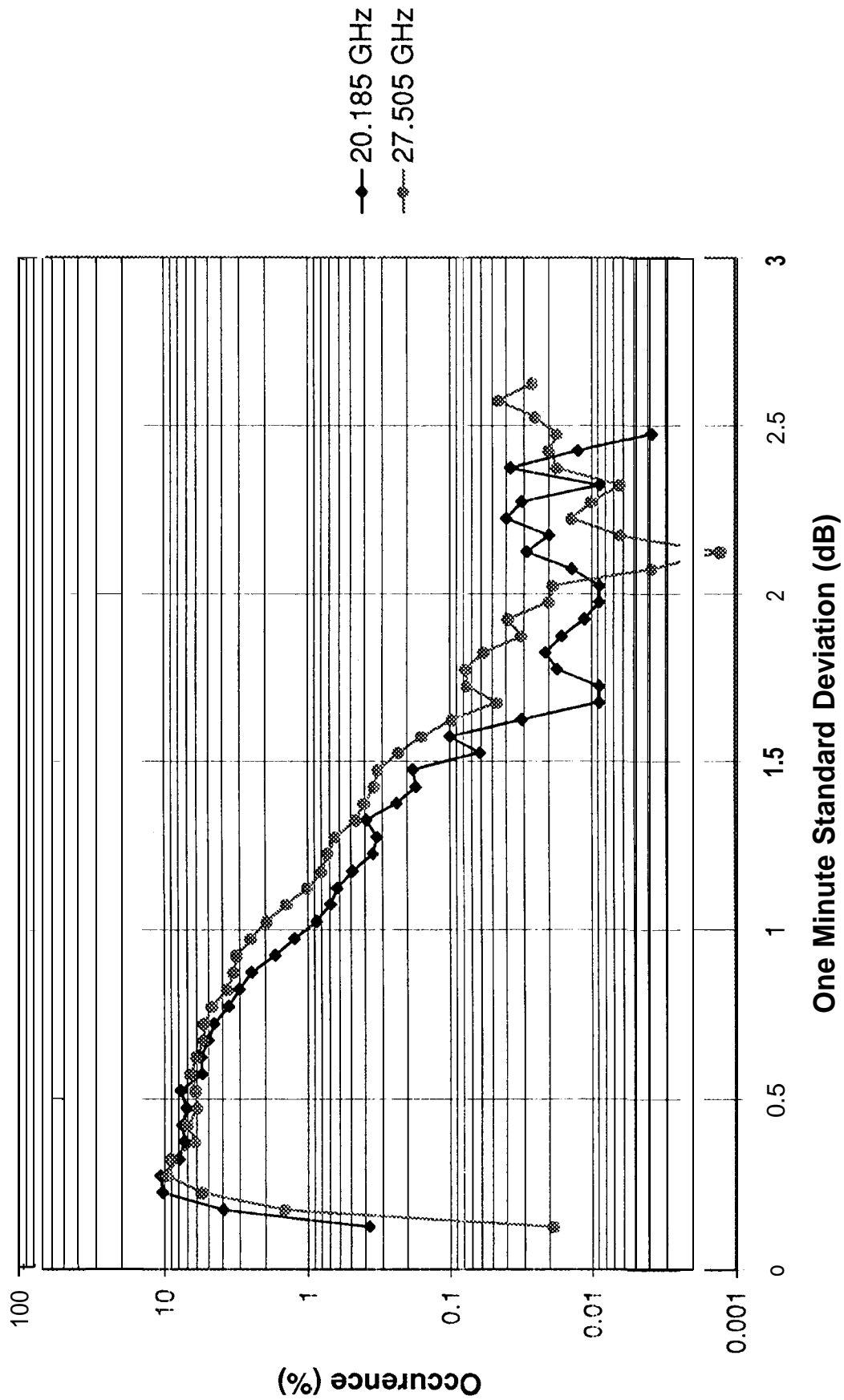


Fig. 7. One Minute Standard Deviation PDF
8/1 6/94



**Fig. 8. One Minute Standard Deviation PDF
August 1994**

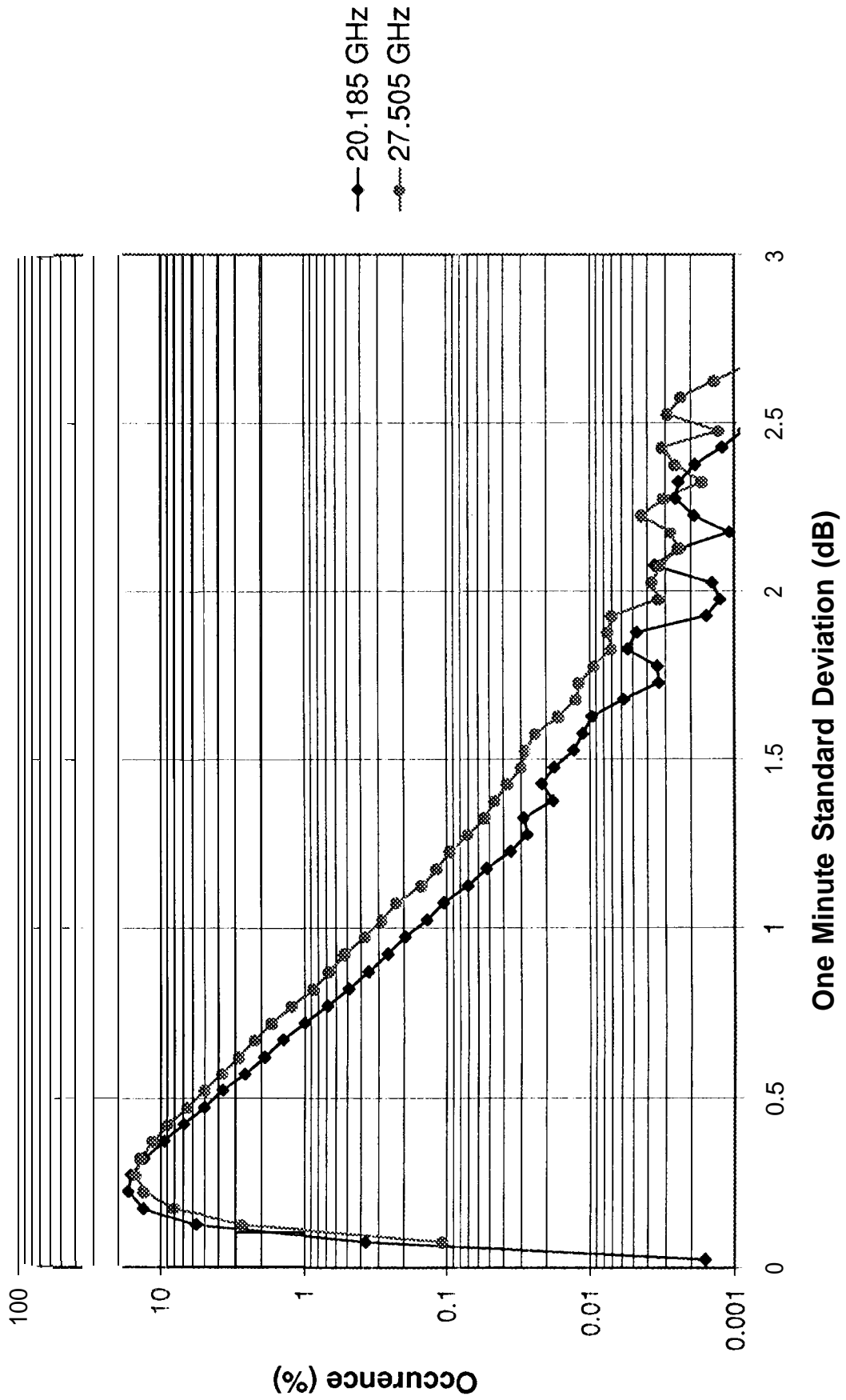


Fig. 9. Probability Density Function of Hourly Standard Deviation

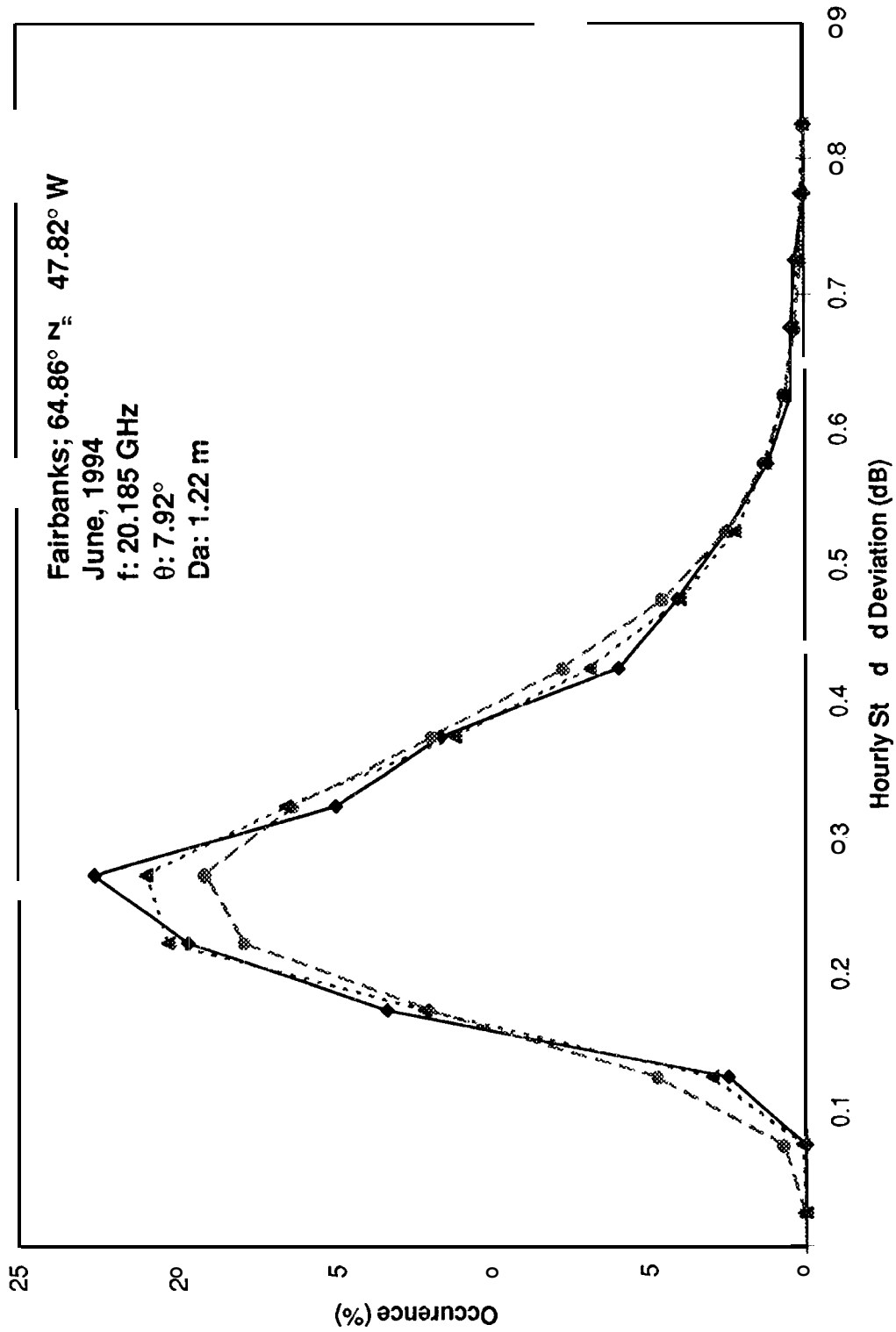


Fig. 10. Probability Density Function of Hourly Standard Deviation

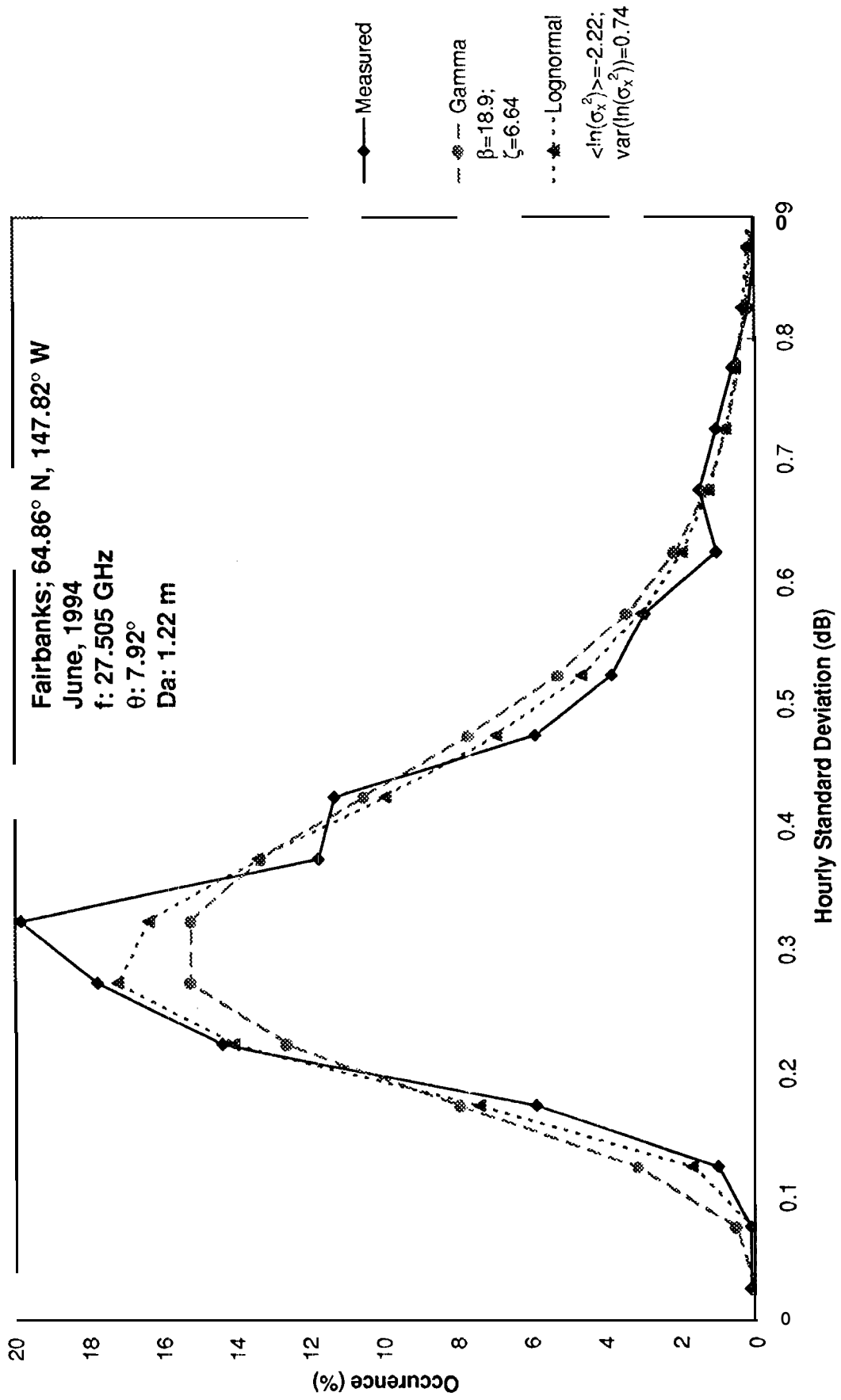


Fig. 11. Annual Variation in Hourly Standard Deviation

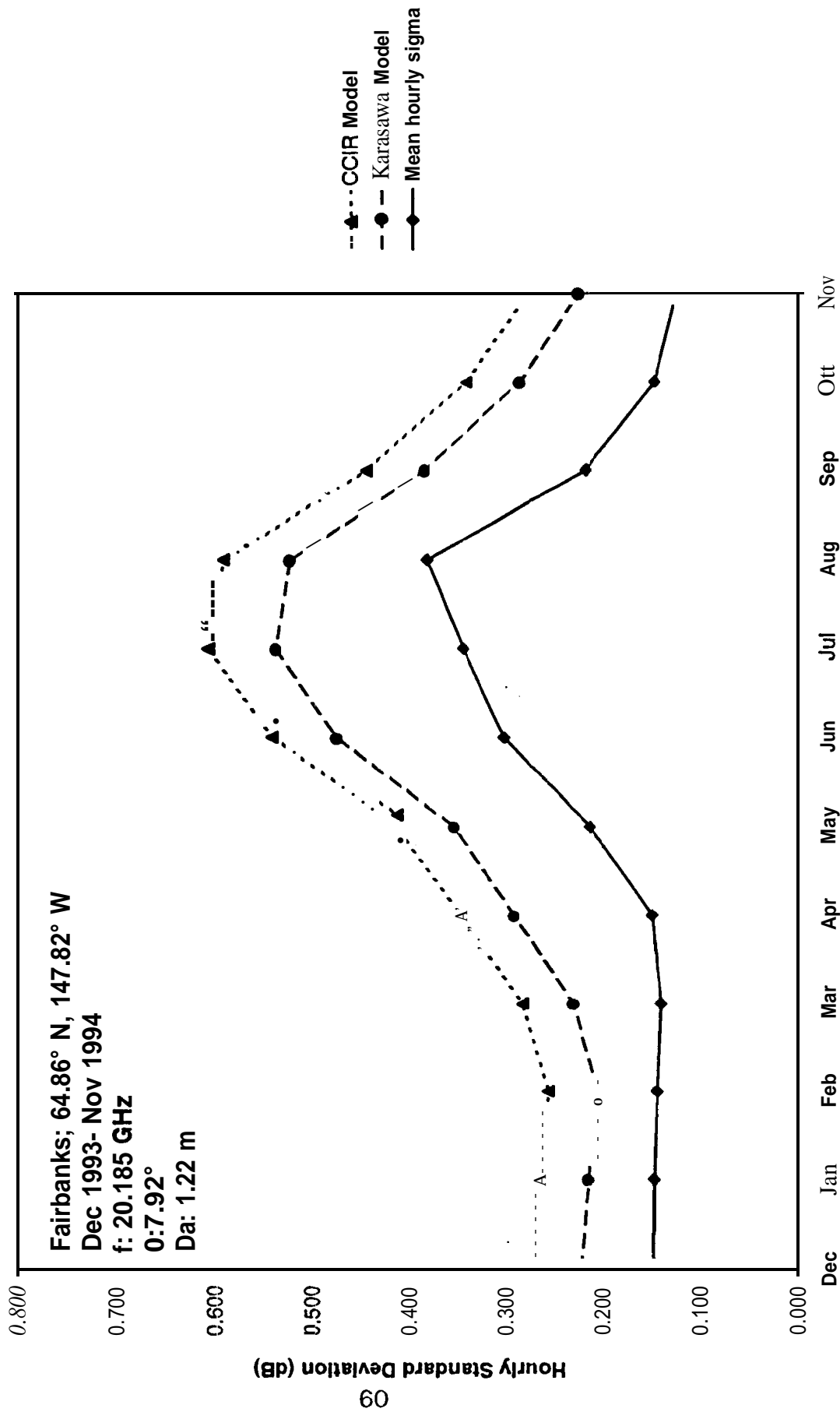
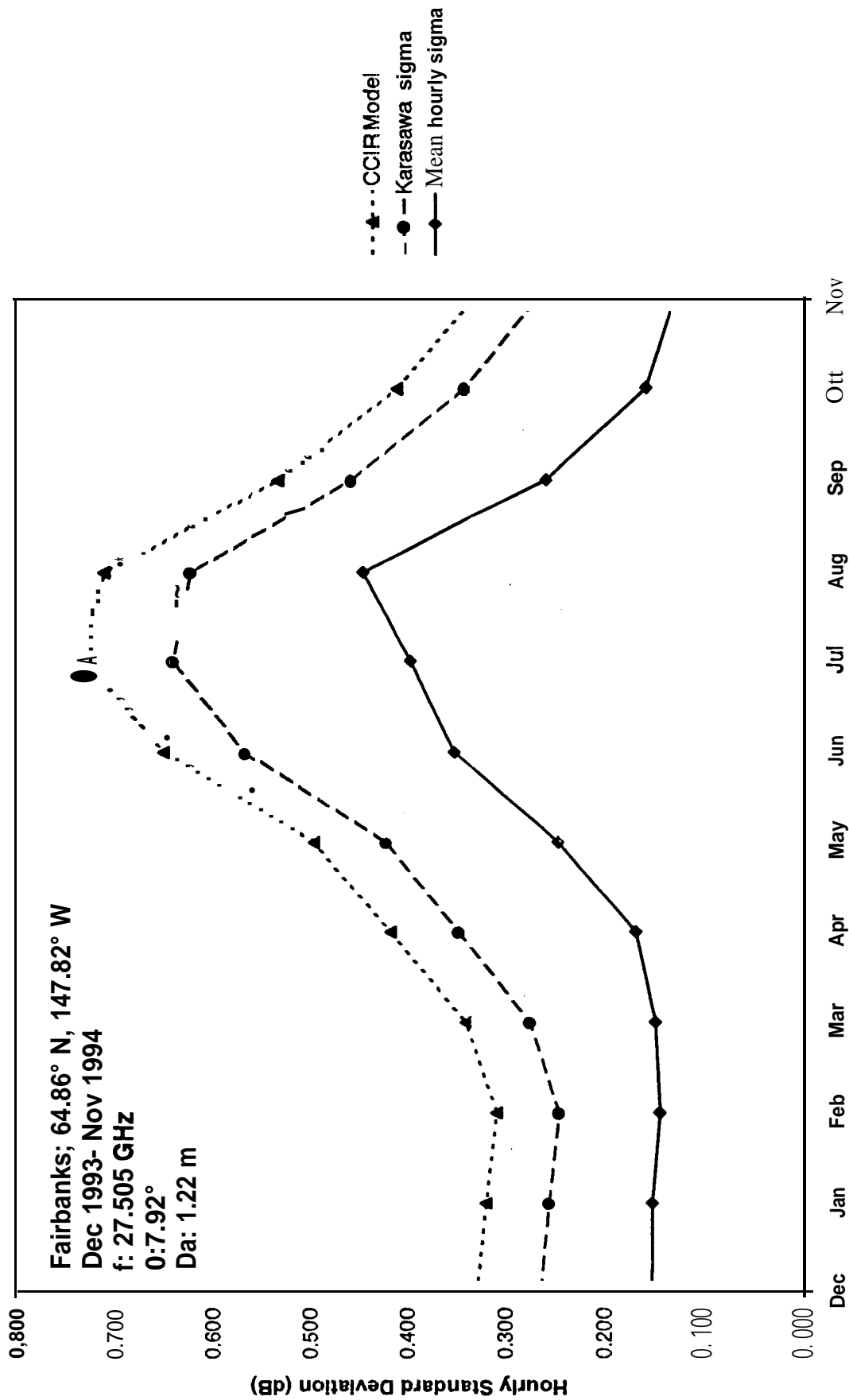


Fig. 12. Annual Variation in Hourly Standard Deviation



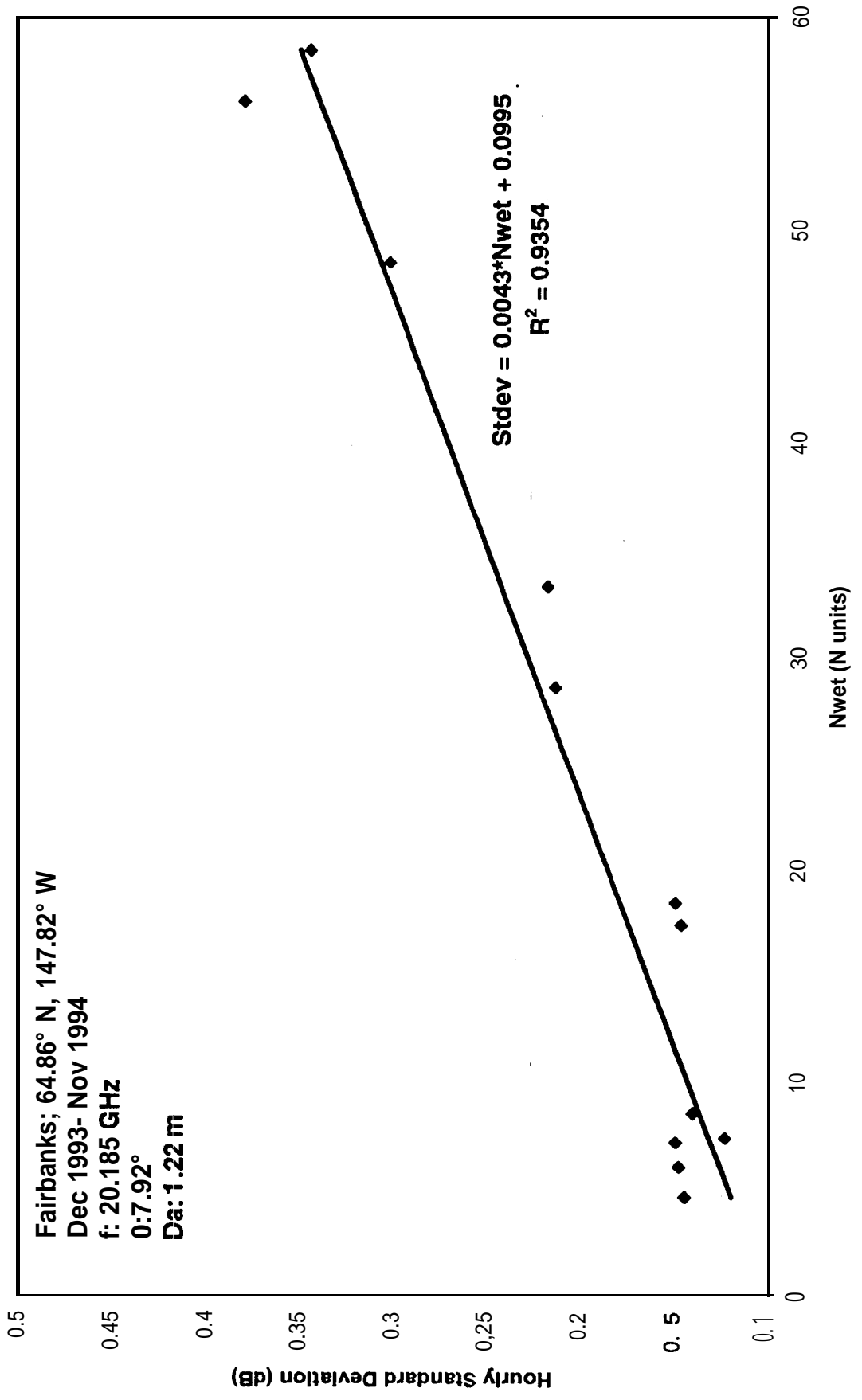


Fig. 14. Linear Regression of Nwet and Hourly Standard Deviation

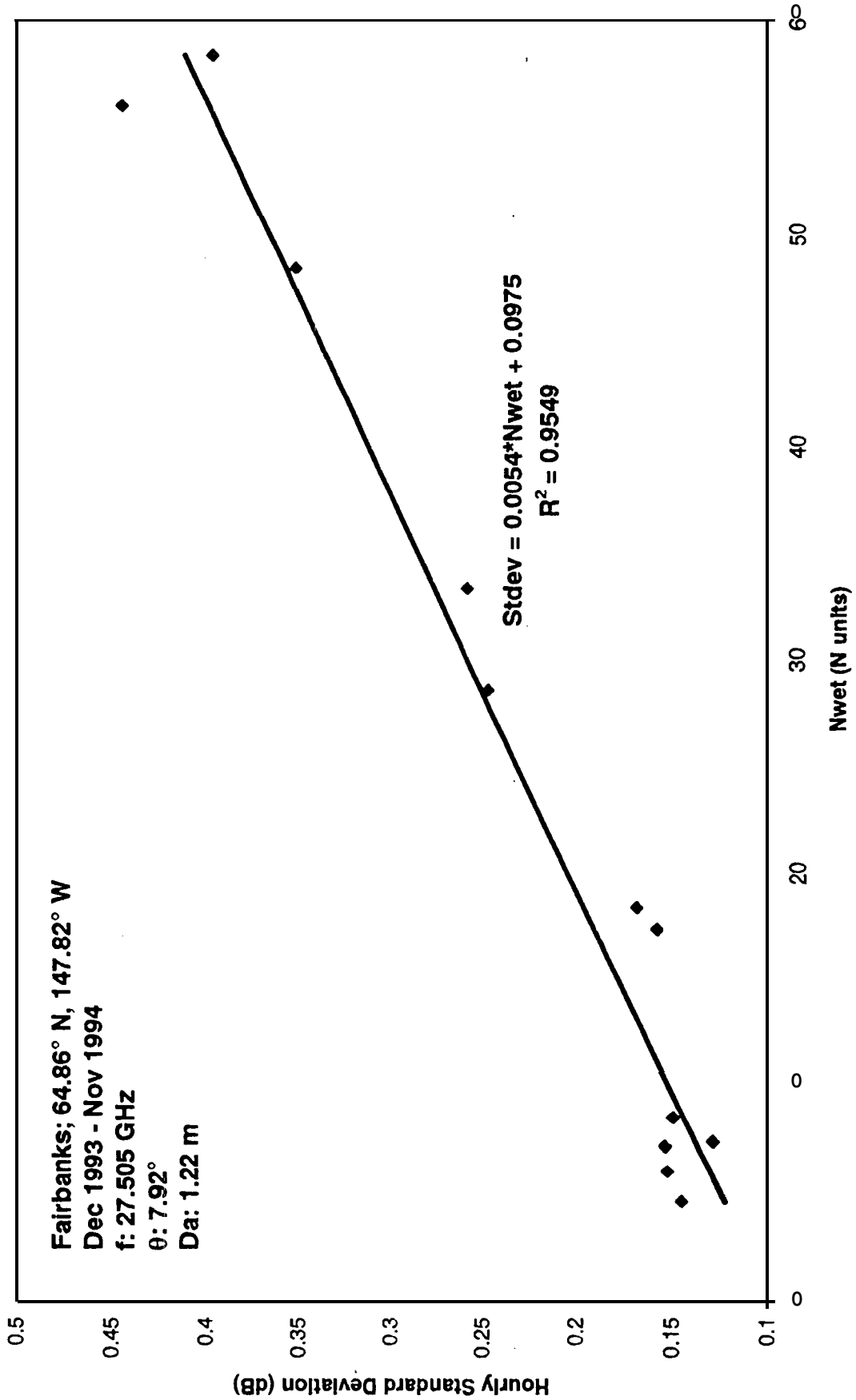


Fig. 15. One Minute Standard Deviation Percentage of Time Functions

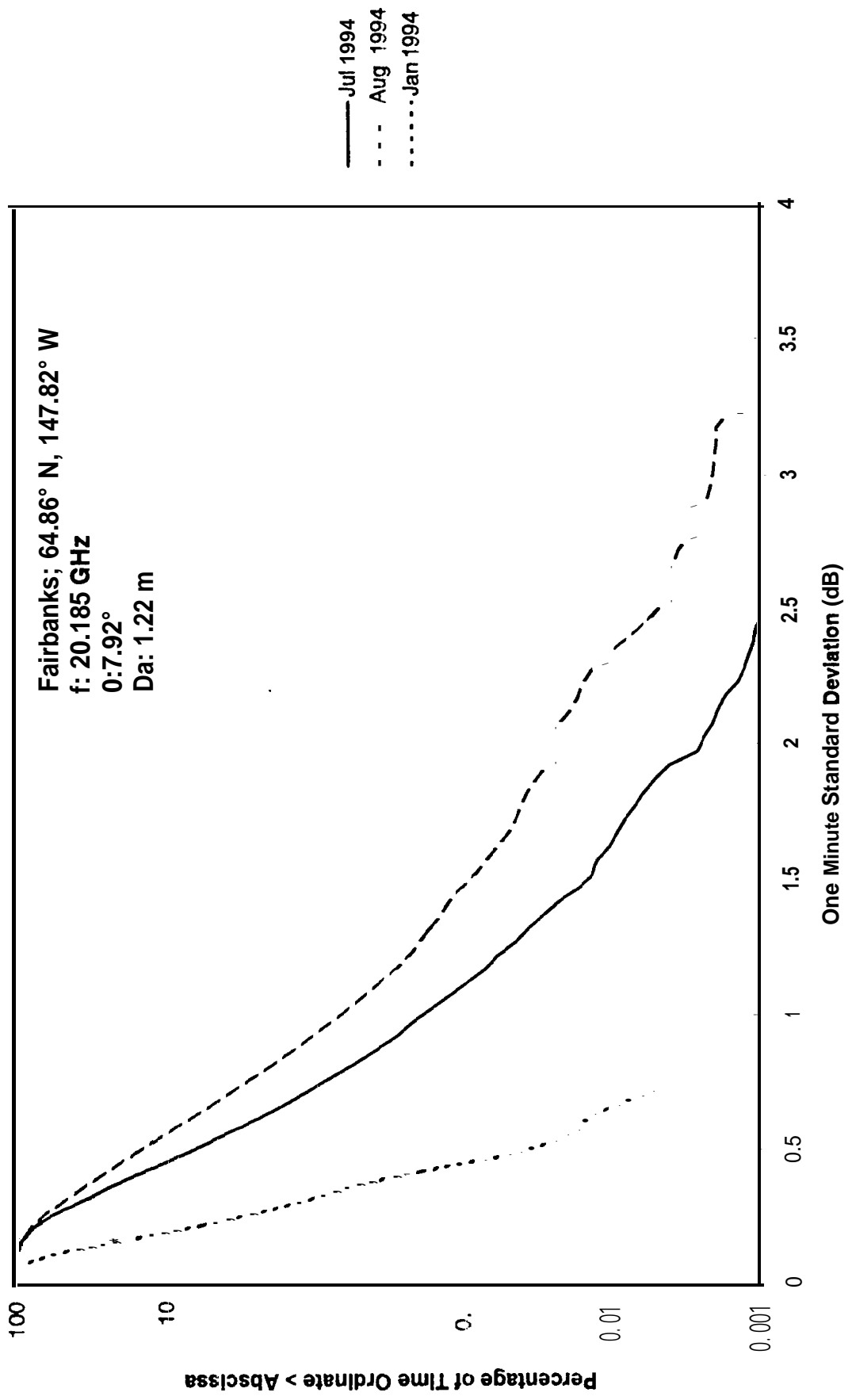
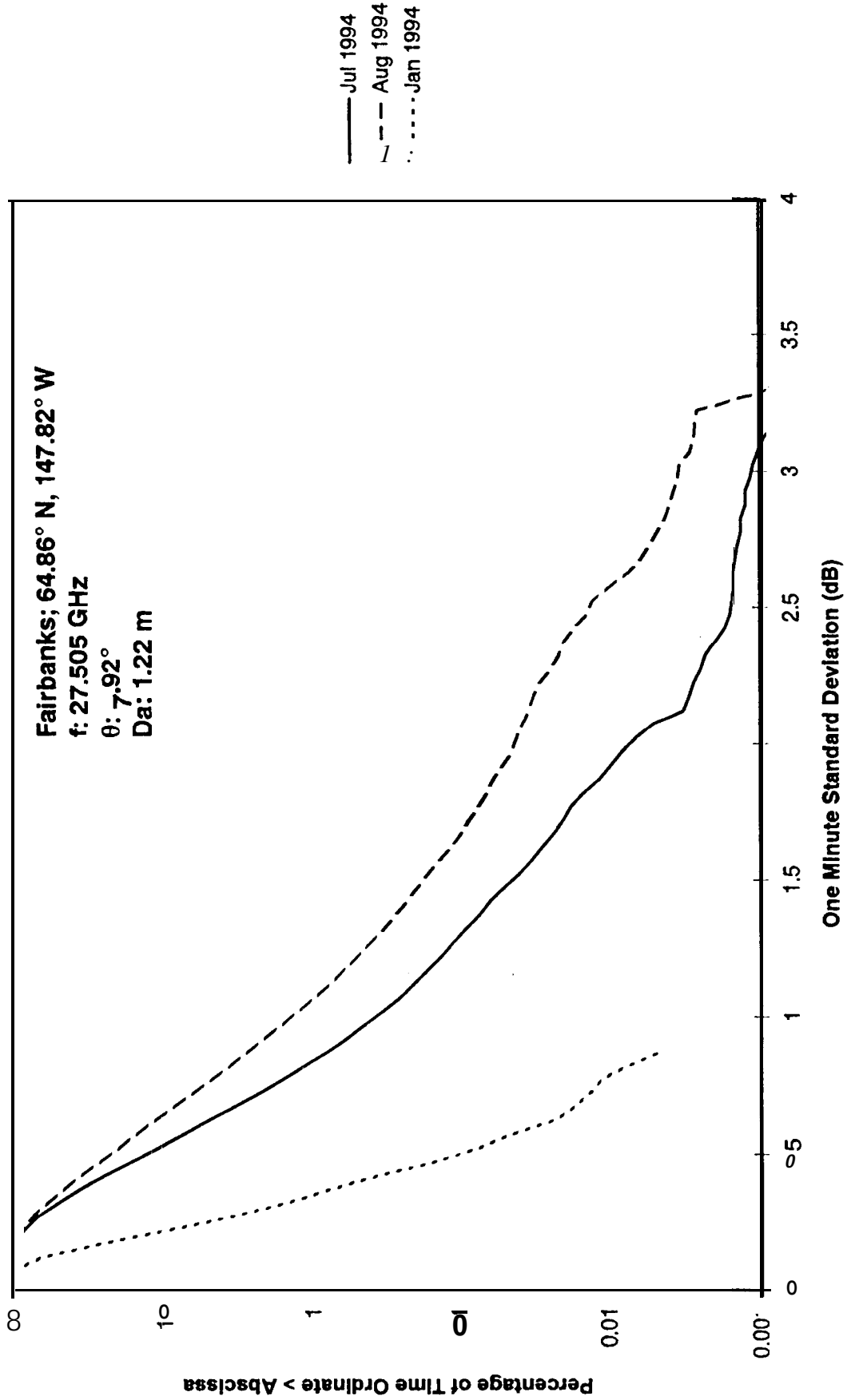


Fig. 16. One Minute Standard Deviation Percent of Time Functions



F ● 7. One Minute Standard Deviation Percent of Time Function

